CHEMISTRY OF MATERIALS

pubs.acs.org/cm

Article

Machine Learning Analysis and Discovery of Zero-Dimensional ns^2 Metal Halides toward Enhanced Photoluminescence Quantum Yield

Maxim S. Molokeev,*,# Binbin Su,# Aleksandr S. Aleksandrovsky, Nicolay N. Golovnev, Mikhail E. Plyaskin, and Zhiguo Xia*

Cite This: *Chem. Mater.* 2022, 34, 537−546

Read Online

ACCESS | Metrics & More | Article Recommendations | Supporting Information

ABSTRACT: The dependence of photoluminescence quantum yield (PLQY) on the crystal structure of existing zero-dimensional ns^2 metal halides is analyzed with the help of principal component analysis and random forest methods. The primary role of the distance between metal ions in different compounds is revealed, and the influence of other structural features such as metal-halogen distance and the distortion of metal-halogen polyhedrons are quantified. Accordingly, the two previously unknown Sb^{3+}-based zero-dimensional metal halides were synthesized to verify the obtained model. Experimental studies of the two compounds demonstrated good agreement with the predictions, and the PLQY of $(C_{10}H_{16}N)_2SbCl_5$ is found to be 96.5%. *Via* machine learning analysis, we demonstrate that concentration quenching is the main factor that determines PLQY for all s^2 ion metal halides, which will accelerate the discovery of new luminescence metal halides.

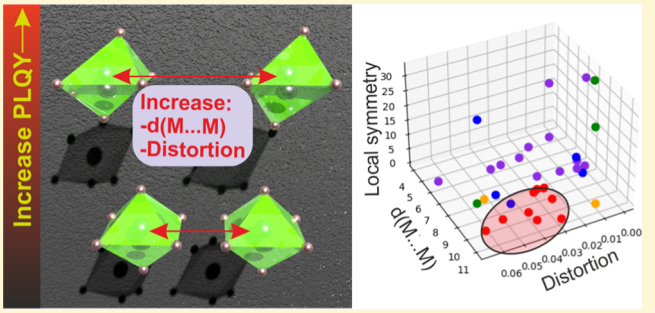

1. INTRODUCTION

Prediction of functional properties of new materials for a wide range of applications before their discovery and experimental synthesis is an important and obviously challenging problem. Nowadays, machine learning (ML) attracted huge interests which employed it to make predictions of different material properties, including whole life cycle of material discovery,[1] searching new synthetic methods,[2] studying new prominent ferroelectric compounds,[3] searching high-temperature ferroelectric perovskites,[4] accurate band gap prediction,[5] metamaterial design,[6] space group determination,[7−9] and so on. However, the majority of areas still lack satisfactory predictive tools. One of such areas is the area of science concerning luminescent materials. Certain progress is achieved in solution of a somehow simplified task, namely, the prediction of optical properties, commonly absorption, from structural data obtained for a certain material after its actual synthesis.[10] The progress in prediction of luminescent properties of new materials is much more modest than in the case of absorption since a set of factors influencing the luminescent properties are very diversified and hardly coverable using modern *ab initio* computer simulation tools.

Recently, zero-dimensional (0D) ns^2 luminescent metal halides have attracted tremendous interests due to their specific electronic and optical properties. Among these new types of materials, a number of highly luminescent ones with photoluminescence quantum yield (PLQY) approaching unity were discovered,[11−13] while other cognate materials with a seemingly insignificant difference in chemical content demonstrate a drastic drop in PLQY that could not be satisfactorily explained.[14−19] Thus, it is meaningful to establish the relationship between the structure and high PLQY, which will accelerate the design of new materials with functional applications and greatly promote the development of 0D luminescent metal halides. Recently, the joint work by our group demonstrated that concentration quenching is a decisive factor influencing PLQY of Mn^{2+}-based hybrid metal halides.[20] Simultaneously, the same result was obtained by Mao *et al.*[21] who established that a Mn···Mn distance of 9 Å guarantees PLQY above 13% in the class of compounds investigated in ref 21. In these studies, a series of materials with differing concentration quenching are synthesized and completely characterized to reach the conclusion formulated above. However, concerning all 0D hybrid metal halides with ns^2 metal ions, including Pb^{2+}, Sn^{2+}, Sb^{3+}, and Bi^{3+}, the emission is mainly originated from the typical self-trapped excitons (STEs), which is closely related to metal halide units in their structures.[12,13,22−24] Influence of concentration quenching was mentioned only for Pb^{2+} in 0D *trans*-$[Pb(DMTU\text{-}S)_4Cl_2]$[25]

Received: August 8, 2021
Revised: December 29, 2021
Published: January 11, 2022

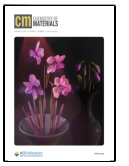

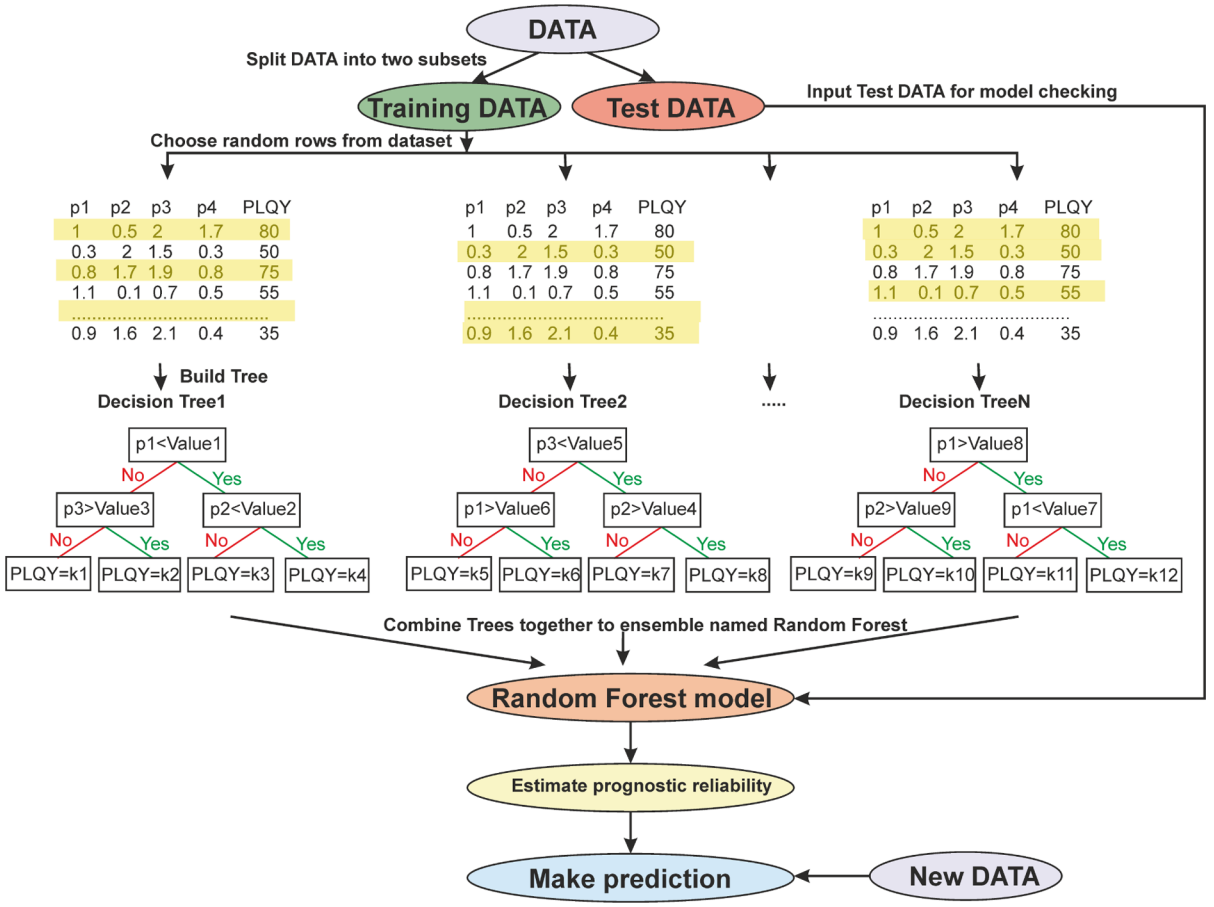

Figure 1. Main process of RF building, checking, and making prediction. Herein, the collected data initially were divided into training and test data sets with 80:20 proportions. The bootstrap aggregation algorithm was used for creating multiple different models from a single training data set. The ensemble of trees combined together has a name RF. After that test data were used to check reliability of RF model for prediction. Finally, the new data can be used to make prediction of desired PLQY property.

that belongs to a different coordination class of compounds than those which will be studied in the present paper; Pb···Pb distance 9.4 Å was established to prevent from concentration quenching in ref 25. Thus, the PLQY is mainly affected by the environment of central metal ions, such as the distance of metal ion, local symmetry, ability to form hydrogen bonds to the organic cations, and so on. However, so far, there is no design principle on the prediction and discovery of new luminescent zero-dimensional metal halides with high PLQY. Considering the costly synthesis and characterization of an extremely large set of compounds, it is anticipated to analyze already existing data and then to establish the relationship between structural type and PLQY in ns^2 metal halides.

Presently, one of the well-known methods of machine learning for the property prediction is deep learning (DL); however, it should be stressed that thousands of data samples should be supplied in this case and a lot of time will be spent for data collection.[26−31] Moreover, there is the so-called "supervised" algorithm, which demands tuning of hyperparameters in order to obtain good and correct prediction on new data. In addition, DL acts as the so-called "black-box", that is, it gives information about predicted values without revealing the rules because weight distribution between hidden neuron layers cannot be interpreted. Therefore, scientists usually use other ML methods, such as Naive Bayesian (NB) learning, random forest (RF), *and so forth.*[31−42] The NB method assigns class labels from some finite set to problem instances, represented as vectors of feature values. Therefore, it is not appropriate for some tasks with continuous class values, that is, for regression analysis. The RF method is an ensemble learning method (Figure 1) for classification, regression, and other tasks, and it is invariant under scaling and various other transformations of feature values, is robust to inclusion of irrelevant features, and produces inspectable models.[43] The RF result can be easily showed and even interpreted. Moreover, RF can be used to rank the importance of feature variables (Figure S1) in a regression or classification problem in a natural way, which is a very important tool for analysis and deriving structure−property rules. In the present work, we will use this method together with principal component analysis (PCA) to obtain some "structure−property" relations, namely, relationships between the structure and PLQY, which is one of the main characteristics of luminescent materials. PCA is also a good tool to select main structural components which can be used to simplify input parameters for ML and make training procedure more stable and robust. Finally, we used RF for training and prediction purposes, and it showed very good results with the discovery of new compounds with high PLQY.

2. EXPERIMENTAL SECTION

2.1. Reagents. 1,3-Cyclohexanedimethanamine ($C_8H_{18}N_2$, 98%), benzyltrimethylammonium chloride ($C_{10}H_{16}NCl$, 98%), antimony chloride ($SbCl_3$, 99%), *N*,*N*-dimethylformamide (DMF, 99%), and ethylalcohol (95%) were purchased from Aladdin. HCl aqueous

https://doi.org/10.1021/acs.chemmater.1c02725
Chem. Mater. 2022, 34, 537−546

Table 1. Data Set of 0D Hybrid Metal Halides and Inorganic Metal Halides, and the Predicted Values Were Obtained from the RF Model

M	compounds	measured PLQY (%)	predicted PLQY (%)	difference (%)	reference
Sb^{3+}	$((C_6H_5)_4P)_2SbCl_5$	87	87	0	23
	$(C_{11}H_{13}N_2)_3SbCl_6$	87.5	85	2.5	14
	$(C_{11}H_{13}N_2)_2SbCl_5$	22.3	38	−15.7	14
	$(C_8H_{15}N_2)_2SbCl_5$	86.3	78	8.3	47
	$(C_8H_{20}N)_2SbCl_5$	86	71	15	48
	$(C_{13}H_{22}N)_2SbCl_5$	98	73	25	48
	$(C_{36}H_{30}NP_2)_2SbCl_5$	98.1	94	4.1	49
	$(C_6H_8N_2O_2)_3SbCl_6$	55	50	5	52
	$(C_7H_{10}N)_3SbBr_6$	1	3	−2	15
Sn^{2+}	$(C_4N_2H_{14}Br)_4SnBr_6$	95	89	6	50
	$(C_4N_2H_{14}I)_4SnI_6$	75	77	−2	13
	$(C_{10}H_{22}N)_2SnBr_4$	75	66	9	51
	$(C_9NH_{20})_2SnBr_4$	46	56	−10	12
	$[(C_8H_{12}N)_4SnBr_6][C_8H_{12}NBr]_2[CCl_2H_2]_2$	90	88	2	52
	$(C_8H_{14}N_2)_2SnBr_6$	40	56	−16	19
	$(C_8H_{12}N)SnBr_4$	0.1	1.6	−1.5	62
	$(C_6N_2H_{16}Cl)_2SnCl_6$	8.1	9	−0.9	16
	Cs_4SnBr_6	20	21	−1	53
Pb^{2+}	$(C_9NH_{20})_6Pb_3Br_{12}$	12	18	−6	54
	$(C_{13}H_{19}N_4)_2PbBr_4$	40	57	−17	17
	$(C_{10}H_{22}N)_2PbBr_4$	24	34	−10	51
	$(C_3H_{12}N_2)PbBr_4$	0.5	3	−2.5	58
	$(C_6H_{14}N)_2PbBr_4$	9	8	1	59
	$(C_6H_{18}O_2N_2)PbBr_4$	9	7	2	58
	$(C_6H_{18}O_2N_2)PbCl_4$	2	5	−3	58
	$(C_9H_{20}N)_9(ZnCl_4)_2Pb_3Cl_{11}$	100	82	18	11
	$(C_4N_2H_{14})PbBr_4$	1.7	3	−1.3	60
	$(C_3H_{11}N_3O)_2PbBr_6(H_2O)_4$	9.2	24	−14.8	61
	Cs_4PbBr_6	45	49	−4	55
Bi^{3+}	$(C_{18}H_{24}Bi_2Cl_{12}K_2N_2O_6)(C_9H_8NO)_2(H_2O)_2$	18	41	−23	56
	$(C_7H_{10}N)BiBr_6$	1	4	−3	15
	$Cs_3Bi_2Br_9$	29.6	20	−9.6	57
	mean ± standard deviation	42.8 ± 36.4	43.6 ± 31.8	−1.4 ± 10.1	
	$(C_8H_{20}N_2)SbCl_5$[a]	18.8	6.5	−12.3	this work
	$(C_{10}H_{16}N)_2SbCl_5$[a]	96.5	75.9	20.6	this work

[a]New compounds under investigation were not used to build the RF model. The PLQY estimation was made for them using the model.

solution (38% in water by weight) was purchased from Sinopharm Chemical Reagent Co., Ltd. All reagents and solvents were used without further purification.

2.2. Synthesis. $(C_8H_{20}N_2)SbCl_5$ single crystals were synthesized by the saturated crystallization method. First, 1 mmol $C_8H_{18}N_2$ and 1 mmol $SbCl_3$ were dissolved in 10 mL of HCl at 100 °C for 10 min to form a clear solution. The large sheet single crystals that were colorless transparent were obtained by slowly evaporating the HCl solution at room temperature for a few days. Finally, the obtained single crystals were washed with ethanol and dried in vacuum at 60 °C overnight. Powder crystals (Figure S2) were obtained by evaporating the HCl solution at 80 °C for a few minutes. For $(C_{10}H_{16}N)_2SbCl_5$ single crystals, $C_{10}H_{16}NCl$ (2 mmol) and $SbCl_3$ (1 mmol) were first dissolved in DMF (15 mL) at room temperature with stirring to form a clear solution. Then, large-sized crystals were obtained by slowly evaporating the solvent at room temperature for a few days. Powder crystals were obtained by evaporating the solvent at 60 °C for a few minutes.

2.3. Characterization. Single-crystal X-ray diffraction (SCXRD) of $(C_8H_{20}N_2)SbCl_5$ and $(C_{10}H_{16}N)_2SbCl_5$ was collected using an XtaLAB AFC12 four-circle single-crystal diffractometer (Rigaku) equipped with a CCD detector, graphite monochromator, and Mo Kα radiation source (λ = 1.5406 Å) at 150 K. The orientation matrix and cell parameters were defined and refined for the set of 38450 and 35647 reflections for $(C_8H_{20}N_2)SbCl_5$ and $(C_{10}H_{16}N)_2SbCl_5$, respectively. The unit cells $(C_8H_{20}N_2)SbCl_5$ and $(C_{10}H_{16}N)_2SbCl_5$ correspond to orthorhombic and monoclinic symmetry, respectively. Space groups *Pbca* and *Pn* were determined from the statistical analysis of the intensities of all the reflections. The absorption corrections were applied using the CrysAlisPro program. The structures were solved by the direct methods using package SHELXT and refined in the anisotropic approach for nonhydrogen atoms using SHELXL program.[44] All the hydrogen atoms of the organic ligands were positioned geometrically as riding on their parent atoms with d(C−H) = 0.97 Å for the C−H bonds and d(N−H) = 0.89 Å for all other N−H bonds and $U_{iso}(H) = 1.2U_{eq}(C,N)$. The structural tests for the presence of missing symmetry elements and possible voids were produced using the PLATON program.[45] The photoluminescence (PL) and photoluminescence excitation (PLE) spectra were obtained on an FLS1000 fluorescence spectrophotometer (Edinburgh Instruments Ltd., U. K.) The photoluminescence quantum yields (PLQYs) were recorded using a sphere, which was attached to the FLS1000 spectrofluorometer. The PLQYs were calculated based on the equation: $\eta_{QE} = I_S/(E_R - E_S)$, in which I_S is the luminescence emission photon number of the sample, E_R represents the photon number of the excitation light of the empty integrated sphere, and E_S is the excitation photon number of the excited sample.

https://doi.org/10.1021/acs.chemmater.1c02725
Chem. Mater. 2022, 34, 537−546

Table 2. Structural Parameters Used to Build the RF Model for Prediction

compound	d(M−X) average, Å	MX_n distortion	d(M···M), Å	local symmetry of M site	reference
$((C_6H_5)_4P)_2SbCl_5$	2.5348	0.0533	10.0049	2	23
$(C_{11}H_{13}N_2)_3SbCl_6$	2.6609	0.0259	9.5133	1	14
$(C_{11}H_{13}N_2)_2SbCl_5$	2.5283	0.0110	8.8928	10	14
$(C_8H_{15}N_2)_2SbCl_5$	2.5572	0.0290	8.5036	1	47
$(C_8H_{20}N)_2SbCl_5$	2.5581	0.0276	8.9417	3	48
$(C_{13}H_{22}N)_2SbCl_5$	2.5722	0.0312	8.6708	1	48
$(C_{36}H_{30}NP_2)_2SbCl_5$	2.5682	0.0292	11.0421	1	49
$(C_6H_8N_2O_2)_3SbCl_6$	3.0288	0.0250	5.8795	1	52
$(C_7H_{10}N)_3SbBr_6$	2.8119	0.0245	7.6457	1	15
$(C_4N_2H_{14}Br)_4SnBr_6$	3.0525	0.0626	10.207	1	50
$(C_4N_2H_{14}I)_4SnI_6$	3.2193	0.0105	10.7464	1	13
$(C_{10}H_{22}N)_2SnBr_4$	2.7977	0.0553	8.4218	3	51
$(C_9NH_{20})_2SnBr_4$	2.7979	0.0595	8.5597	3	12
$[(C_8H_{12}N)_4SnBr_6][C_8H_{12}NBr]_2\ [CCl_2H_2]_2$	2.9920	0.0400	9.8901	1	52
$(C_8H_{14}N_2)_2SnBr_6$	2.9913	0.0045	8.3700	1	19
$(C_8H_{12}N)SnBr_4$	3.0717	0.0205	5.9157	4	62
$(C_6N_2H_{16}Cl)_2SnCl_6$	2.4256	0.0046	7.7765	3	16
Cs_4SnBr_6	2.6387	0	7.6155	30	53
$(C_9NH_{20})_6Pb_3Br_{12}$	3.0312	0.0002	4.0897	16	54
$(C_{13}H_{19}N_4)_2PbBr_4$	2.8627	0.0443	8.9526	1	17
$(C_{10}H_{22}N)_2PbBr_4$	2.8672	0.0493	8.4235	3	51
$(C_3H_{12}N_2)PbBr_4$	3.0420	0.0409	6.0917	1	58
$(C_6H_{14}N)_2PbBr_4$	2.8512	0.0069	5.4004	3	59
$(C_6H_{18}O_2N_2)PbBr_4$	2.8980	0.0392	10.5787	1	58
$(C_6H_{18}O_2N_2)PbCl_4$	2.8792	0.0133	7.7772	1	58
$(C_9H_{20}N)_9(ZnCl_4)_2Pb_3Cl_{11}$	3.0239	0.0354	5.9770	1	11
$(C_4N_2H_{14})PbBr_4$	3.0109	0.0020	8.1354	2	60
$(C_3H_{11}N_3O)_2PbBr_6(H_2O)_4$	2.7195	0.00002	8.6309	17	61
Cs_4PbBr_6	2.7381	0	8.4363	32	55
$(C_{18}H_{24}Bi_2Cl_{12}K_2N_2O_6)(C_9H_8NO)_2(H_2O)_2$	2.7105	0.0066	8.1633	2	56
$(C_7H_{10}N)BiBr_6$	3.0036	0.0661	5.7805	1	15
$Cs_3Bi_2Br_9$	2.8461	0.0469	5.9587	19	57
mean ± standard deviation	2.82 ± 0.27	0.027 ± 0.020	8.09 ± 1.68	5.3 ± 8.2	
$(C_8H_{20}N_2)SbCl_5$[a]	2.7367	0.1075	3.797	1	this work
$(C_{10}H_{16}N)_2SbCl_5$[a]	2.7586	0.0256	8.935	1	this work

[a]New compounds under investigation were not used to build the RF model. The PLQY estimations were made for them using the model.

3. DATA AND METHOD

3.1. Data Set Description. The data set of 0D metal halides studied here contains 32 compounds (29 hybrid metal halides and 3 inorganic metal halides). The descriptive statistics and the plot of the considered data set are summarized in Tables 1 and 2 and Figure S3, respectively. The selected structural parameters in Table 2 were considered as main featured parameters, which have the biggest influence on PLQY values. The first parameter "d(M−X) average" equals to the average value of M−X bond lengths from the first coordination sphere of M ions (M = Pb^{2+}, Sn^{2+}, Sb^{3+}, and Bi^{3+}). The second parameter "MX_n distortion" equals to the distortions of isolated MX_n polyhedrons, which were calculated using the following formula[46]

$$D = \frac{1}{n}\sum_{i=1}^{n}\frac{l_i - l_{av}}{l_{av}}$$

where l_i is the distance from the central atom to the ith coordinating atom and l_{av} is the average bond length. The third parameter "d(M···M)" is just the shortest distance between M ions in the structure, and this parameter should be associated with the concentration quenching mechanism. The last parameter is "local symmetry of M site" which equals to the number associated with the point group (Table S1) of Wyckoff positions of M ions.

Preliminary data analysis revealed that PLQY values of compounds showed almost uniform distribution, which means that all representative compounds were selected. The local symmetry of M ions in compounds showed the maximum around 0−1 which is a normal situation because hybrid halides usually crystallize in low space group symmetry (P-1, $P2_1/c$, and $C2/c$) and M ions are often located in general sites. It should be noted that d(M···M) distribution also showed one maximum at 8−9 Å which could be an important parameter because most of these compounds show luminescence.

3.2. Principal Component Analysis. PCA is a multivariate method that converts several correlated variables into several linearly uncorrelated variables named principal components. In this conversion, the first principal components contain the most information about the data set.[63] It should be noted that numerous variables ($N > 3$), which span N-dimensional space, cannot be visualized, and it is hard to analyze data. If N parameters can be reduced to 2 or 3 principal components without large loss of information, then it can be easily represented and analyzed.

https://doi.org/10.1021/acs.chemmater.1c02725
Chem. Mater. 2022, 34, 537−546

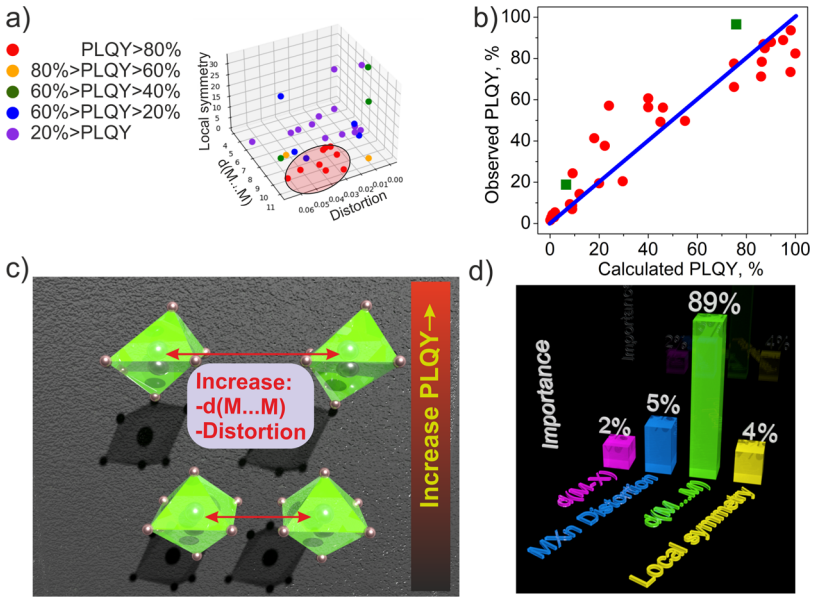

Figure 2. (a) Samples with high PLQY values (red circles in highlighted area) are segregated from others in the 3D space spanned on three most important parameters. (b) Comparative plot of observed PLQY values per calculated PLQY obtained from the RF model. Linear fit proves correctness of the model. Green bars marked new compounds under investigation. (c) Importance of four feature parameters on PLQY values in the RF model. The *d*(M···M) distance has the major influence. (d) Model describes possible ways to increase PLQY values in 0D halides: increase distance between M···M ions and increase distortion associated with lowering of local symmetry.

This very feature was used in our case. To build the PCA models in our study, we used simple self-written python script (see the Supporting Information) using the Python 3.6 programming language.[64] The standard libraries were used to write the program: numpy, pandas, sklearn, and xlwt. Initially, we tested several models with different numbers of structural parameters (bonds, angles, coordination numbers, *etc.*), which were further converted to three parameters by PCA. We accepted only models for which loss is no more than 20% of the initial information after PCA data reducing. One of the models with four parameters listed in Table 2 can be converted to tree parameters' model without strong information loss (less than 20%). The plot which contains all 32 compounds in 3D space of PCA-converted parameters (*x*,*y*,*z*) is depicted in Figure S4. The most important fact is that compounds with high PLQY values were segregated from compounds with low PLQY (highlighted red area in Figure S4). It means that PLQY values really correlate with suggested structural parameters, and the predictive model is built. The PCA model can be used to make prediction, for example, four parameters can be extracted from the new structure, after that converted to (*x*,*y*,*z*) PCA parameters, and plotted in Figure S4. If the new point falls into the red area, then it means that the new compound with high probability will have high PLQY. However, this method cannot estimate approximate values of PLQY and requires much effort. The easiest way is to build a model based on the machine learning method and use it for prediction. The deep learning method should be excluded because it requires thousands of data examples for learning. The RF method is an unsupervised algorithm that can work well with limited sets of data; therefore, it was selected for our purpose to build the prediction model.

3.3. RF Method. The prediction tool used in this study is RF, an ensemble method based on regression trees.[65] The regression trees are built by recursive binary partitioning of the multidimensional predictor space into regions by constructing a multitude of "decision trees" at training time and outputting the class that is the "mode" of the classes (classification) or mean/average prediction (regression) of the individual trees.[66] Predictions are performed by passing new data parameters from the root through the internal nodes until a terminal node is reached. We used simple self-written python script named RandomForest.py (see the Supporting Information) using the Python 3.6 programming language[57,65] in order to build the described RF model. The standard libraries were used in the program: numpy, pandas, sklearn, matplotlib, and mpl_toolkits. Since this machine learning algorithm is stochastic, we used it with averaging performance across ten repeats of cross-validation. Each time, the data were split into the two random data sets: a set for training procedure (80% of total data) and another set for test (20% of total data). The mean absolute error (MAE) of training set and test set PLQY values measured in this way was 6.4 and 16.4%, respectively. Additionally, we have made fivefold cross-validation test on the whole data set, which showed MAE = 15 ± 5%. Previously obtained MAE values are within two estimated standard deviations from the mean of this value. The reliability and precision of prediction can be increased further by increasing the number of observed data. However, currently, the main correlation between the structure and property was revealed using 32 compounds only (Figure 2a,b).

The calculated PLQY values and their differences from the observed ones were less than 10% (Table 2, Figure S5), and good fit between them can be checked in Figure 2b. An additional RF model using only one input parameter *d*(M···M) was also built (Figure S6). The MAE of training set and test set PLQY values becomes 7.0 and 26.4%, respectively, and fivefold cross-validation test on the whole data set showed MAE = 18 ± 5% which is worse. Comparison of Figures 2b and S6 allows understanding how the employment of the extended set of parameters improves the correlation between training set and prognostic dependence. The RF model can now be used to

https://doi.org/10.1021/acs.chemmater.1c02725
Chem. Mater. 2022, 34, 537−546

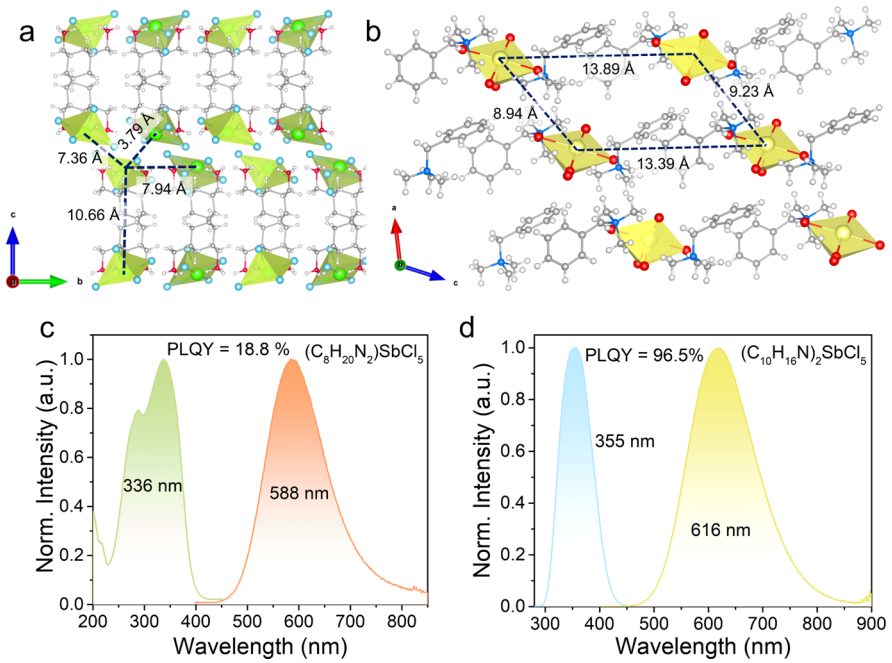

Figure 3. (a) Crystal structure of $(C_8H_{20}N_2)SbCl_5$; Sb···Sb distances: 3.79 Å (shortest), 7.36, 7.94, and 10.66 Å labeled with black dashes. (b) Crystal structure of $(C_{10}H_{16}N)_2SbCl_5$; Sb···Sb distances: 8.94 Å (shortest), 9.23, 13.39, and 13.89 Å labeled with black dashes. (c,d) Normalized photoluminescence excitation (PLE) and emission spectra of $(C_8H_{20}N_2)SbCl_5$ and $(C_{10}H_{16}N)_2SbCl_5$, respectively.

predict PLQY of any 0D hybrid or inorganic halides. We prepared several new compounds, whose structure was successfully resolved. Their structures allow us to forecast PLQY values using the RF model and compare these values with the real ones.

It should be noted that RF allows measuring the importance of the feature after training. The selected value is permuted among the training data and the error is computed on this perturbed data set. The importance score for the selected feature is computed by averaging the difference in error before and after the permutation over all trees.[67] The score is normalized by the standard deviation of these differences. Features which produce large values for this score are ranked as more important than features which produce small values. We performed this analysis also and found correlation with PCA analysis.

4. RESULTS AND DISCUSSION

The several interesting results were obtained using PCA and RF methods with PLQY data of 0D halides. First of all, the PCA method really shows the existence of "structure−property" relations for these compounds, and several rules can be derived. For example, three linearly uncorrelated principal components (x,y,z) fit 87% of all data, and their contributions are 45% for x; 26% for y; and 16% for z component. According to Figure S4, the x value should be the smallest (negative), the z value should be the biggest (positive) in order to reach high PLQY, and the y value almost has no influence. According to calculated eigenvectors (Table S2), one can see that the coefficient associated with d(M···M) has simultaneously big reduction in the x value and large increase in the z value under increasing d(M···M). Therefore, the main structural feature which increases PLQY is increasing d(M···M) values. Moreover, the decreasing local symmetry leads to simultaneous reduction in the x value and increase in z; therefore, this is an additional mechanism to control PLQY. Increasing polyhedron MX_n distortion, which has some correlation with decreasing M local symmetry, also has a positive influence on PLQY. The d(M−X) parameter has not so pronounced linear influence on the PLQY value because the corresponding eigenvector component has six times smaller influence on the x value in comparison with other structural parameters under consideration (Table S2). The importance of feature parameters was calculated from the RF model also and the result is depicted in Figure 2c. One can see that the d(M···M) distance has the major influence on PLQY and MX_n polyhedron distortion and lowering of local symmetry have the second and third places, respectively. All samples were presented in 3D space of these three parameters (Figure 2a) and high PLQY samples were segregated from others, forming a small area. In general, the mechanism of structural transformation, which on average should increase PLQY values, is depicted in Figure 2d. It is important to stress that obtained rules should work with M = Pb^{2+}, Sn^{2+}, Sb^{3+}, and Bi^{3+} and with any possible organic molecules in the compound, that is it covers a relatively broad range of halides. Moreover, the simple method demonstrated in the present work can help to reveal many other "structure−property" relations for other crystal families.

Second, the RF model was built, which can quickly estimate PLQY values. In order to prove its reliability, we synthesized two new 0D metal halides, the crystal structures are shown in Figure 3a,b. The main crystal data are shown in Table S3. The crystallographic data are deposited in Cambridge Crystallographic Data Centre (CCDC 2102048-2102049). The data can be downloaded from the site (www.ccdc.cam.ac.uk/data_request/cif). The PL and PLE and PLQYs of $(C_8H_{20}N_2)SbCl_5$ and $(C_{10}H_{16}N)_2SbCl_5$ are shown in Figure 3c,d. We calculated the PLQY values of new crystal structures of $(C_8H_{20}N_2)SbCl_5$ and $(C_{10}H_{16}N)_2SbCl_5$ and compared them with the as-measured PLQY values in the laboratory (Table 1). In order to use the RF model, we take structural parameters from the

https://doi.org/10.1021/acs.chemmater.1c02725
Chem. Mater. 2022, 34, 537−546

CIF files: average M-X distance, polyhedron distortion, shortest Me···Me distance, and local symmetry (Table 2). These parameters were uploaded to the RF model and predicted PLQY values were calculated using routine procedure of averaging the Forest voting: 6.5 and 75.9% for $(C_8H_{20}N_2)SbCl_5$ and $(C_{10}H_{16}N)_2SbCl_5$, respectively. The difference of the measured and predicted values appeared to be −12.3 and −20.6% (Table 1), which are close to the obtained MAE value (15%), and actually not very large proving good prediction reliability. It should be noted that we have got good predicative result using only four structural parameters and, namely, they are responsible for structure−property relationships. Moreover, experiments with new crystals showed that both high PLQY and low PLQY values can be predicted with a similar error. Therefore, the as-obtained RF model can be used to screen many CIF files to find compounds with high/low PLQY and select desirable materials among them before using routine synthesis procedure. Screening of current CSD database and predicting PLQY values of structures revealed compounds with average or low PLQY values only, not high PLQY. This is because the data set we used is not representative of the structures in CSD, so that it took a lot of time to find compounds with high PLQY in order to make a balanced data set. The discovery of a new material with a PLQY as high as 96.5% was a very lucky and not related with prediction program at this time. However, understanding main parameters which influence PLQY can help to build new compounds with high luminescence.

Let us finally obtain a rough estimate for "average" Förster radius of dipole−dipole energy transfer between s^2 ions in the group of materials under study. For this purpose, the dependence of PLQY on the interionic distance can be fitted by the curve describing the inverse probability of the excited ion to experience energy transfer instead of radiative decay (Figure 4). One can see from Figure 4 that rough agreement

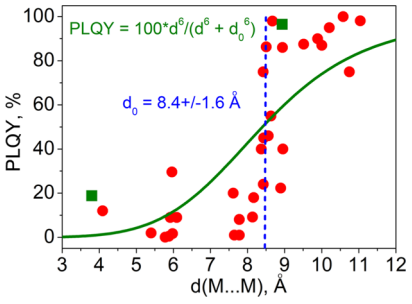

Figure 4. "Average" Förster radius d_0 estimation from the complete data set of compounds and fitting using formula PLQY = 100 × $d^6/(d^6 + d_0^6)$, where d is the shortest M···M distance. Fitting revealed that value d_0 = 8.4 Å segregates all samples into two classes with high and low values of PLQY, respectively. It appeared that Förster radii for all samples included in the data set are, as the first approximation, just the same.

can be obtained with the chosen fitting, and rough estimate for the Förster radius is 8.4 Å. In reality, every ion must have its own value of Förster radius that may have minor variations in dependence on the organic/inorganic host. As seen from Figure 4 Förster radii for all cases included in the data set are, as the first approximation, just the same. Influence of concentration quenching for s^2 electronic system is, therefore, in general slightly weaker than for the d^5 electronic system investigated in refs 20 and 21.

5. CONCLUSIONS

In conclusion, we demonstrate that a relatively small data set of hybrid and inorganic metal halides is sufficient for machine learning analysis of luminescent properties of these materials, including making predictions and deriving "structure−property" relationships and PLQY. The PCA analysis with eigenvectors was used to reveal rules to increase/control PLQY, and these rules can be used to design new luminescence materials with prominent PLQY values. It was shown that PLQY of 0D halides with M = Pb^{2+}, Sn^{2+}, Sb^{3+}, and Bi^{3+} ions increases with the increase in M···M average distance, decrease in M local symmetry, and increase in MX_n polyhedron distortion. The RF unsupervised algorithm with splitting data on training and test sets and averaging performance across ten repeats of cross-validation was used in order to foresee PLQY values from a structure. Several new compounds were tested using a suggested model and very good agreement was observed, and the model and methodology developed herein will be used to accelerate the discovery of new luminescence metal halides with high PLQY.

■ ASSOCIATED CONTENT

Supporting Information

The Supporting Information is available free of charge at https://pubs.acs.org/doi/10.1021/acs.chemmater.1c02725.

PCA result, RF model, main crystal structural parameters for selected compounds, experimental and simulated XRD patterns, and main parameters of selected compounds (PDF)

Crystallographic information of $(C_8H_{20}N_2)SbCl_5$ (CIF)

Crystallographic information of $(C_{10}H_{16}N)_2SbCl_5$ (CIF)

PCA.py—self-written python script for principal component analysis, RandomForest.py—self-written python script for RF analysis, Data.xlsx—data with collected samples used for PCA.py and RandomForest.py, and Predict.xlsx—data of new samples for estimation their PLQY (ZIP)

■ AUTHOR INFORMATION

Corresponding Authors

Maxim S. Molokeev − *Laboratory of Crystal Physics, Kirensky Institute of Physics, Federal Research Center KSC SB RAS, Krasnoyarsk 660036, Russia; Siberian Federal University, Krasnoyarsk 660041, Russia; Research and Development Department, Kemerovo State University, Kemerovo 650000, Russia;* orcid.org/0000-0002-8297-0945; Email: msmolokeev@mail.ru

Zhiguo Xia − *The State Key Laboratory of Luminescent Materials and Devices, Guangdong Provincial Key Laboratory of Fiber Laser Materials and Applied Techniques, School of Materials Science and Engineering and School of Physics and Optoelectronics, South China University of Technology, Guangzhou 510641, China;* orcid.org/0000-0002-9670-3223; Email: xiazg@scut.edu.cn

Authors

Binbin Su − *The State Key Laboratory of Luminescent Materials and Devices, Guangdong Provincial Key Laboratory of Fiber Laser Materials and Applied Techniques, School of Materials Science and Engineering, South China University of Technology, Guangzhou 510641, China*

Aleksandr S. Aleksandrovsky − *Laboratory of Coherent Optics, Kirensky Institute of Physics, Federal Research Center KSC SB RAS, Krasnoyarsk 660036, Russia; Siberian Federal University, Krasnoyarsk 660041, Russia;* orcid.org/0000-0003-1821-6718

Nicolay N. Golovnev − *Siberian Federal University, Krasnoyarsk 660041, Russia*

Mikhail E. Plyaskin − *Laboratory of Crystal Physics, Kirensky Institute of Physics, Federal Research Center KSC SB RAS, Krasnoyarsk 660036, Russia; Siberian Federal University, Krasnoyarsk 660041, Russia*

Complete contact information is available at: https://pubs.acs.org/10.1021/acs.chemmater.1c02725

Author Contributions

#M.S.M. and B.S. contributed equally to this work.

Notes

The authors declare no competing financial interest.

■ ACKNOWLEDGMENTS

This work is supported by the National Natural Science Foundation of China (51961145101 and 51972118), International Cooperation Project of National Key Research and Development Program of China (2021YFE0105700), Guangzhou Science and Technology Project (202007020005), and the Local Innovative and Research Teams Project of Guangdong Pearl River Talents Program (2017BT01X137). This work is also funded by RFBR according to the research project no. 19-52-80003.

■ REFERENCES

(1) Li, J.; Lim, K.; Yang, H.; Ren, Z.; Raghavan, S.; Chen, P.-Y.; Buonassisi, T.; Wang, X. AI Applications through the Whole Life Cycle of Material Discovery. *Matter* **2020**, *3*, 393−432.

(2) Zahrt, A. F.; Henle, J. J.; Rose, B. T.; Wang, Y.; Darrow, W. T.; Denmark, S. E. Prediction of Higher-Selectivity Catalysts by Computer-Driven Workflow and Machine Learning. *Science* **2019**, *363*, 6424.

(3) Li, Q.; Nelson, C. T.; Hsu, S.-L.; Damodaran, A. R.; Li, L.-L.; Yadav, A. K.; McCarter, M.; Martin, L. W.; Ramesh, R.; Kalinin, S. V. Quantification of flexoelectricity in PbTiO3/SrTiO3 superlattice polar vortices using machine learning and phase-field modeling. *Nat. Commun.* **2017**, *8*, 1468.

(4) Balachandran, P. V.; Kowalski, B.; Sehirlioglu, A.; Lookman, T. Experimental Search for High-Temperature Ferroelectric Perovskites Guided by Two-Step Machine Learning. *Nat. Commun.* **2018**, *9*, 1668.

(5) Rajan, A. C.; Mishra, A.; Satsangi, S.; Vaish, R.; Mizuseki, H.; Lee, K.-R.; Singh, A. K. Machine-Learning-Assisted Accurate Band Gap Predictions of Functionalized MXene. *Chem. Mater.* **2018**, *30*, 4031−4038.

(6) Bessa, M. A.; Glowacki, P.; Houlder, M. Bayesian Machine Learning in Metamaterial Design: Fragile Becomes Supercompressible. *Adv. Mater.* **2019**, *31*, No. e1904845.

(7) Ziletti, A.; Kumar, D.; Scheffler, M.; Ghiringhelli, L. M. Insightful Classification of Crystal Structures Using Deep Learning. *Nat. Commun.* **2018**, *9*, 2775.

(8) Liu, C.-H.; Tao, Y.; Hsu, D.; Du, Q.; Billinge, S. J. L. Using a Machine Learning Approach to Determine the Space Group of a Structure from the Atomic Pair Distribution Function. *Acta Crystallogr., Sect. A: Found. Crystallogr.* **2019**, *75*, 633−643.

(9) Azarapin, N. O.; Aleksandrovsky, A. S.; Atuchin, V. V.; Gavrilova, T. A.; Krylov, A. S.; Molokeev, M. S.; Mukherjee, S.; Oreshonkov, A. S.; Andreev, O. V. Synthesis, structural and spectroscopic properties of orthorhombic compounds BaLnCuS3 (Ln = Pr, Sm). *J. Alloys Compd.* **2020**, *832*, 153134.

(10) Ferrari, A. M.; Orlando, R.; Rérat, M. Ab Initio Calculation of the Ultraviolet-Visible (UV-vis) Absorption Spectrum, Electron-Loss Function, and Reflectivity of Solids. *J. Chem. Theory Comput.* **2015**, *11*, 3245−3258.

(11) Zhou, C.; Lin, H.; Neu, J.; Zhou, Y.; Chaaban, M.; Lee, S.; Worku, M.; Chen, B.; Clark, R.; Cheng, W.; Guan, J.; Djurovich, P.; Zhang, D.; Lü, X.; Bullock, J.; Pak, C.; Shatruk, M.; Du, M.-H.; Siegrist, T.; Ma, B. Green Emitting Single-Crystalline Bulk Assembly of Metal Halide Clusters with Near-Unity Photoluminescence Quantum Efficiency. *ACS Energy Lett.* **2019**, *4*, 1579−1583.

(12) Zhou, C.; Lin, H.; Shi, H.; Tian, Y.; Pak, C.; Shatruk, M.; Zhou, Y.; Djurovich, P.; Du, M. H.; Ma, B. A Zero-Dimensional Organic Seesaw-Shaped Tin Bromide with Highly Efficient Strongly Stokes-Shifted Deep-Red Emission. *Angew. Chem., Int. Ed.* **2018**, *57*, 1021−1024.

(13) Zhou, C.; Lin, H.; Tian, Y.; Yuan, Z.; Clark, R.; Chen, B.; van de Burgt, L. J.; Wang, J. C.; Zhou, Y.; Hanson, K.; Meisner, Q. J.; Neu, J.; Besara, T.; Siegrist, T.; Lambers, E.; Djurovich, P.; Ma, B. Luminescent Zero-Dimensional Organic Metal Halide Hybrids with Near-Unity Quantum Efficiency. *Chem. Sci.* **2018**, *9*, 586−593.

(14) Wang, Z.; Zhang, Z.; Tao, L.; Shen, N.; Hu, B.; Gong, L.; Li, J.; Chen, X.; Huang, X. Hybrid Chloroantimonates(III): Thermally Induced Triple-Mode Reversible Luminescent Switching and Laser-Printable Rewritable Luminescent Paper. *Angew. Chem., Int. Ed.* **2019**, *58*, 9974−9978.

(15) Chen, D.; Dai, F.; Hao, S.; Zhou, G.; Liu, Q.; Wolverton, C.; Zhao, J.; Xia, Z. Crystal structure and luminescence properties of lead-free metal halides (C6H5CH2NH3)3MBr6 (M = Bi and Sb). *J. Mater. Chem. C* **2020**, *8*, 7322−7329.

(16) Song, G.; Li, M.; Yang, Y.; Liang, F.; Huang, Q.; Liu, X.; Gong, P.; Xia, Z.; Lin, Z. Lead-Free Tin(IV)-Based Organic-Inorganic Metal Halide Hybrids with Excellent Stability and Blue-Broadband Emission. *J. Phys. Chem. Lett.* **2020**, *11*, 1808−1813.

(17) Lin, H.; Zhou, C.; Chaaban, M.; Xu, L.-J.; Zhou, Y.; Neu, J.; Worku, M.; Berkwits, E.; He, Q.; Lee, S.; Lin, X.; Siegrist, T.; Du, M.-H.; Ma, B. Bulk Assembly of Zero-Dimensional Organic Lead Bromide Hybrid with Efficient Blue Emission. *ACS Mater. Lett.* **2019**, *1*, 594−598.

(18) Chen, D.; Hao, S.; Zhou, G.; Deng, C.; Liu, Q.; Ma, S.; Wolverton, C.; Zhao, J.; Xia, Z. Lead-Free Broadband Orange-Emitting Zero-Dimensional Hybrid (PMA)3InBr6 with Direct Band Gap. *Inorg. Chem.* **2019**, *58*, 15602−15609.

(19) Su, B.; Song, G.; Molokeev, M. S.; Lin, Z.; Xia, Z. Synthesis, Crystal Structure and Green Luminescence in Zero-Dimensional Tin Halide (C8H14N2)2SnBr6. *Inorg. Chem.* **2020**, *59*, 9962−9968.

(20) Zhou, G.; Liu, Z.; Huang, J.; Molokeev, M. S.; Xiao, Z.; Ma, C.; Xia, Z. Unraveling the Near-Unity Narrow-Band Green Emission in Zero-Dimensional Mn2+-Based Metal Halides: A Case Study of (C10H16N)2Zn1-xMnxBr4 Solid Solutions. *J. Phys. Chem. Lett.* **2020**, *11*, 5956−5962.

(21) Mao, L.; Guo, P.; Wang, S.; Cheetham, A. K.; Seshadri, R. Design Principles for Enhancing Photoluminescence Quantum Yield in Hybrid Manganese Bromides. *J. Am. Chem. Soc.* **2020**, *142*, 13582−13589.

(22) Zhou, C.; Xu, L. J.; Lee, S.; Lin, H.; Ma, B. Recent Advances in Luminescent Zero-Dimensional Organic Metal Halide Hybrids. *Adv. Opt. Mater.* **2020**, *9*, 2001766.

(23) Zhou, C.; Worku, M.; Neu, J.; Lin, H.; Tian, Y.; Lee, S.; Zhou, Y.; Han, D.; Chen, S.; Hao, A.; Djurovich, P. I.; Siegrist, T.; Du, M.-H.; Ma, B. Facile Preparation of Light Emitting Organic Metal Halide Crystals with Near-Unity Quantum Efficiency. *Chem. Mater.* **2018**, *30*, 2374−2378.

(24) McCall, K. M.; Morad, V.; Benin, B. M.; Kovalenko, M. V. Efficient Lone-Pair-Driven Luminescence: Structure-Property Relationships in Emissive 5s2 Metal Halides. *ACS Mater. Lett.* **2020**, *2*, 1218−1232.

(25) Golovnev, N. N.; Aleksandrovsky, A. S.; Gerasimova, M. A.; Tomilin, F. N.; Mironov, V. A.; Demina, A. V.; Xia, Z.; Molokeev, M. S. Luminescent Zero-Dimensional Hybrid Lead Thiohalide Nano-

structures for High Quantum Yield and Broadband Excitation. *ACS Appl. Nano Mater.* **2021**, *4*, 3654−3663.
(26) Chen, Y. Q.; Xue, Y. A Deep Learning Approach to Human Activity Recognition Based on Single Accelerometer. *IEEE International Conference on Systems, Man, and Cybernetics*; IEEE, 2015; pp 1488−1492.
(27) Brahimi, M.; Boukhalfa, K.; Moussaoui, A. Deep Learning for Tomato Diseases: Classification and Symptoms Visualization. *Appl. Artif. Intell.* **2017**, *31*, 299−315.
(28) Mundhenk, T. N.; Konjevod, G.; Sakla, W. A.; Boakye, K. A Large Contextual Dataset for Classification, Detection and Counting of Cars with Deep Learning. *Lect. Notes Comput. Sci.* **2016**, *9907*, 785−800.
(29) Feng, S.; Zhou, H.; Dong, H. Using Deep Neural Network with Small Dataset to Predict Material Defects. *Mater. Des.* **2019**, *162*, 300−310.
(30) Fujisawa, Y.; Otomo, Y.; Ogata, Y.; Nakamura, Y.; Fujita, R.; Ishitsuka, Y.; Watanabe, R.; Okiyama, N.; Ohara, K.; Fujimoto, M. Deep-learning-based, computer-aided classifier developed with a small dataset of clinical images surpasses board-certified dermatologists in skin tumour diagnosis. *Br. J. Dermatol.* **2019**, *180*, 373−381.
(31) Rajpurkar, P.; Park, A.; Irvin, J.; Chute, C.; Bereket, M.; Mastrodicasa, D.; Langlotz, C. P.; Lungren, M. P.; Ng, A. Y.; Patel, B. N. AppendiXNet: Deep Learning for Diagnosis of Appendicitis from A Small Dataset of CT Exams Using Video Pretraining. *Sci. Rep.* **2020**, *10*, 3958.
(32) Russell, S. J.; Norvig, P. *Artificial Intelligence, A Modern Approach*, 2nd ed.; Pearson Education, 2003; Vol. *1*(45), pp 5−32.
(33) Deshpande, V. P.; Erbacher, R. F.; Harris, C. An Evaluation of Naive Bayesian Anti-spam Filtering Techniques; *IEEE Information Assurance Workshop*; IEEE, 2007; p 333.
(34) Chen, J.; Huang, H.; Tian, S.; Qu, Y. Feature selection for text classification with Naïve Bayes. *Expert Syst. Appl.* **2009**, *36*, 5432−5435.
(35) Hand, D. J.; Yu, K. Idiot's Bayes-Not So Stupid After All? *Int. Stat. Rev.* **2001**, *69*, 385−398.
(36) Ham, J.; Yangchi Chen, Y. C.; Crawford, M. M.; Ghosh, J. Investigation of the Random Forest Framework for Classification of Hyperspectral Data. *IEEE Trans. Geosci. Electron.* **2005**, *43*, 492−501.
(37) Wang, Q.; Garrity, G. M.; Tiedje, J. M.; Cole, J. R. Naive Bayesian Classifier for Rapid Assignment of rRNA Sequences into the New Bacterial Taxonomy. *Appl. Environ. Microbiol.* **2007**, *73*, 5261−5267.
(38) Zadrozny, B.; Elkan, C. Obtaining Calibrated Probability Estimates from Decision Trees and Naive Bayesian Classifiers. *ICML* **2001**, *1*, 609−616.
(39) Belgiu, M.; Drăguţ, L. Random Forest in Remote Sensing: A Review of Applications and Future Directions. *ISPRS J Photogramm* **2016**, *114*, 24−31.
(40) Svetnik, V.; Liaw, A.; Tong, C.; Culberson, J. C.; Sheridan, R. P.; Feuston, B. P. Random Forest: a Classification and Regression Tool for Compound Classification and QSAR Modeling. *J. Chem. Inf. Comput. Sci.* **2003**, *43*, 1947−1958.
(41) Breiman, L. Random Forests. *Mach. Learn.* **2001**, *45*, 5−32.
(42) Shi, T.; Horvath, S. Unsupervised Learning With Random Forest Predictors. *J. Comput. Graph Stat.* **2012**, *15*, 118−138.
(43) Hastie, T.; Robert, T.; Friedman, J. *The Elements of Statistical Learning*; Springer-Verlag New York, 2009; p 745.
(44) Sheldrick, G. M. Crystal structure refinement with SHELXL. *Acta Crystallogr., Sect. C: Struct. Chem.* **2015**, *71*, 3−8.
(45) Spek, A. L. Single-crystal structure validation with the program PLATON. *J. Appl. Crystallogr.* **2003**, *36*, 7−13.
(46) Baur, W. H. The Geometry of Polyhedral Distortions. Predictive Relationships for the Phosphate Group. *Acta Crystallogr., Sect. B: Struct. Crystallogr. Cryst. Chem.* **1974**, *30*, 1195−1215.
(47) Wang, Z.-P.; Wang, J.-Y.; Li, J.-R.; Feng, M.-L.; Zou, G.-D.; Huang, X.-Y. [Bmim]2SbCl5: a main group metal-containing ionic liquid exhibiting tunable photoluminescence and white-light emission. *Chem. Commun.* **2015**, *51*, 3094−3097.
(48) Li, Z.; Li, Y.; Liang, P.; Zhou, T.; Wang, L.; Xie, R.-J. Dual-Band Luminescent Lead-Free Antimony Chloride Halides with Near-Unity Photoluminescence Quantum Efficiency. *Chem. Mater.* **2019**, *31*, 9363−9371.
(49) He, Q.; Zhou, C.; Xu, L.; Lee, S.; Lin, X.; Neu, J.; Worku, M.; Chaaban, M.; Ma, B. Highly Stable Organic Antimony Halide Crystals for X-Ray Scintillation. *ACS Mater. Lett.* **2020**, *2*, 633−638.
(50) Zhou, C.; Tian, Y.; Wang, M.; Rose, A.; Besara, T.; Doyle, N. K.; Yuan, Z.; Wang, J. C.; Clark, R.; Hu, Y.; Siegrist, T.; Lin, S.; Ma, B. Low-Dimensional Organic Tin Bromide Perovskites and Their Photoinduced Structural Transformation. *Angew. Chem., Int. Ed.* **2017**, *56*, 9018−9022.
(51) Zhou, C.; Zhao, Y.; Yu, T.; Lin, H. R.; Clark, R.; Chen, B. H.; Burgt, L. J.; Wang, J. C.; Hanson, K.; Meisner, Q. J.; Neu, J.; Besara, T.; Siegrist, T.; Lambers, E.; Djurovich, P.; Ma, B. W. Highly Luminescent Bulk Quantum Materials Based on Zero-Dimensional Organic Tin Halide Perovskites. Submission date: 23 Feb 2017, arXiv preprint (Materials Science), 1702.07200, https://arxiv.org/abs/1702.0720, (accessed March 27, 2017).
(52) Xu, L.-J.; Lin, H.; Lee, S.; Zhou, C.; Worku, M.; Chaaban, M.; He, Q.; Plaviak, A.; Lin, X.; Chen, B.; Du, M.-H.; Ma, B. 0D and 2D: The Cases of Phenylethylammonium Tin Bromide Hybrids. *Chem. Mater.* **2020**, *32*, 4692−4698.
(53) Benin, B. M.; Dirin, D. N.; Morad, V.; Wörle, M.; Yakunin, S.; Rainò, G.; Nazarenko, O.; Fischer, M.; Infante, I.; Kovalenko, M. V. Highly Emissive Self-Trapped Excitons in Fully Inorganic Zero-Dimensional Tin Halides. *Angew. Chem., Int. Ed.* **2018**, *57*, 11329−11333.
(54) Zhou, J.; Li, M.; Ning, L.; Zhang, R.; Molokeev, M. S.; Zhao, J.; Yang, S.; Han, K.; Xia, Z. Broad-Band Emission in a Zero-Dimensional Hybrid Organic [PbBr6] Trimer with Intrinsic Vacancies. *J. Phys. Chem. Lett.* **2019**, *10*, 1337−1341.
(55) Zhang, H.; Liao, Q.; Wu, Y.; Chen, J.; Gao, Q.; Fu, H. Pure zero-dimensional Cs4PbBr6 single crystal rhombohedral microdisks with high luminescence and stability. *PCCP* **2017**, *19*, 29092−29098.
(56) Wang, Y.-J.; Xu, L. Synthesis and optical properties of two novel chlorobismuthate(III) complexes: [8-Hydroxyquinolinium]-4K2[BiCl6]2·6H2O (1) and [8-hydroxyquinolinium]6[Bi2Cl10]-[BiCl5(H2O)]·6H2O(2). *J. Mol. Struct.* **2008**, *875*, 570−576.
(57) Lazarini, F. Caesium Enneabromodibismuthate(III). *Acta Crystallogr., Sect. B: Struct. Sci.* **1977**, *33*, 2961−2964.
(58) Dohner, E. R.; Hoke, E. T.; Karunadasa, H. I. Self-assembly of broadband white-light emitters. *J. Am. Chem. Soc.* **2014**, *136*, 1718−1721.
(59) Yangui, A.; Garrot, D.; Lauret, J. S.; Lusson, A.; Bouchez, G.; Deleporte, E.; Pillet, S.; Bendeif, E. E.; Castro, M.; Triki, S.; Abid, Y.; Boukheddaden, K. Optical Investigation of Broadband White-Light Emission in Self-Assembled Organic-Inorganic Perovskite (C6H11NH3)2PbBr4. *J. Phys. Chem. C* **2015**, *119*, 23638−23647.
(60) Yuan, Z.; Zhou, C.; Tian, Y.; Shu, Y.; Messier, J.; Wang, J. C.; van de Burgt, L. J.; Kountouriotis, K.; Xin, Y.; Holt, E.; Schanze, K.; Clark, R.; Siegrist, T.; Ma, B. One-dimensional organic lead halide perovskites with efficient bluish white-light emission. *Nat. Commun.* **2017**, *8*, 14051.
(61) Cui, B. B.; Han, Y.; Huang, B.; Zhao, Y.; Wu, X.; Liu, L.; Cao, G.; Du, Q.; Liu, N.; Zou, W.; Sun, M.; Wang, L.; Liu, X.; Wang, J.; Zhou, H.; Chen, Q. Locally collective hydrogen bonding isolates lead octahedra for white emission improvement. *Nat. Commun.* **2019**, *10*, 5190.
(62) Lin, F.; Wang, H.; Liu, W.; Li, J. Zero-dimensional ionic antimony halide inorganic-organic hybrid with strong greenish yellow emission. *J. Mater. Chem. C* **2020**, *8*, 7300−7303.
(63) Rencher, A. C. *Methods of Multivariate Analysis*; John Wiley & Sons.Inc. Publication, 2002; p 727.
(64) Coelho, L. P.; Richert, W.; Brucher, M. *Building Machine Learning Systems with Python: Explore Machine Learning and Deep Learning Techniques for Building Intelligent Systems Using Scikit-Learn and TensorFlow*; Packt Publishing Ltd., 2018; p 406.
(65) Breiman, L. Random Forests. *Mach. Learn.* **2001**, *45*, 5−32.

(66) Ho, T. K. Random decision forests. In *Proceedings of 3rd International Conference on Document Analysis and Recognition*; Institute of Electrical and Electronics Engineers, 1995; pp 278−282.
(67) Zhu, R.; Zeng, D.; Kosorok, M. R. Reinforcement Learning Trees. *J. Am. Stat. Assoc.* **2015**, *110*, 1770−1784.

https://doi.org/10.1021/acs.chemmater.1c02725
Chem. Mater. 2022, 34, 537−546